ISSN 1063-7834, Physics of the Solid State, 2018, Vol. 60, No. 6, pp. 1061–1067. © Pleiades Publishing, Ltd., 2018.
Original Russian Text © I.I. Musabirov, I.M. Safarov, R.M. Galeyev, R.A. Gaisin, V.V. Koledov, R.R. Mulyukov, 2018, published in Fizika Tverdogo Tela, 2018, Vol. 60, No. 6, pp. 1051–1057.

METALS

Anisotropy of the Thermal Expansion of a Polycrystalline Ni–Mn–Ga Alloy Subjected to Plastic Deformation by Forging

I. I. Musabirov[a,*], I. M. Safarov[a], R. M. Galeyev[a], R. A. Gaisin[a], V. V. Koledov[b], and R. R. Mulyukov[a]

[a] *Institute for Metals Superplasticity Problems, Russian Academy of Sciences, Ufa, 450001 Russia*
[b] *Kotelnikov Institute of Radio Engineering and Electronics, Russian Academy of Sciences, Moscow, 125009 Russia*
**e-mail: irekmusabirov@mail.ru*

Received December 11, 2017

Abstract—The formation of a sharp crystallographic texture in a Ni–Mn–Ga Heusler alloy by the multiple isothermal forging has been studied. An analysis of the thermal expansion near the martensitic transformation temperatures in the as-cast and forged states of the alloy shows that the thermomechanical treatment leads to an increase in the anisotropy of the sample geometric size changing during the phase transformation, which favors an increase in the functional characteristics of the alloy. The structural studies show that the alloy structure after multiple isothermal forging has the bimodal distribution of grain sizes. The formation of the bimodal structure by forging is assumed to make it possible to enhance the stability of the functional properties of the alloy during repeated cycles of the phase transformation.

DOI: 10.1134/S1063783418060240

1. INTRODUCTION

The Heusler alloys belong to promising functional materials due to the ferromagnetic shape memory effect (FSME), the magnetocaloric effect (MCE) and so on, which are observed in the alloys in the region of the martensitic transformation [1–13]. These effects are most strongly observed in single-crystal states of the alloys. For example, the irreversible ferromagnetic shape memory effect in a single-crystal Ni_2MnGa alloy is 11% in magnetic fields up to 1 T [14]. In a polycrystalline state, the effect is, as a rule, one order smaller; but, even in this case, the possibility of applying this effect in practice does not decrease its actuality [15–17]. A lower FSME value in the polycrystalline samples are mainly associated to the grain structure isotropy, which enables the increase in the effect by enhancing the crystallographic texture in the alloy under study. In addition, the existence of internal stresses in the structure is no less of an important factor that favors an increase in the FSME value [6, 18].

The main method of increasing of the anisotropy and crystallographic texture in metals and alloys is a thermomechanical treatment by such methods, for example: rolling [19–24], severe plastic deformation (SPD) [25, 26], multiple isothermal forging (MIF) [27–30], and others. By comparison over other methods of preparing a textured material, for example, the directed crystallization of the melt [31, 32], a substantial advantage of a thermomechanical treatment (TMT) is the simultaneous increase in mechanical properties. In this case, most of the TMT methods which is used to produce new materials with required properties have some disadvantages. For example, rolling and SPD are limited in sizes of final billets of a material obtained as thin plates. In the case of a compressive deformation (upset forging), the modified structure of the billet is inhomogeneous in volume. From this standpoint the MIF method has the most urgency. This method enables to form a required microstructure in a bulk sample with no inhomogeneities inherent to other methods.

It should be noted that there are many publications on the results of studying TMT of Heusler alloys by the methods of rolling [33–37], SPD [38–42], upsetting deformation [43, 44], and extrusion [45]. However, despite the indubitable actuality of studies of the treatment of Heusler alloys by the MIF method, there are no publications on this direction. Based on the above mentioned, the purpose of this work is to reveal the regularities of the influence of TMT by the MIF method of Ni–Mn–Ga alloys on the anisotropy of physical properties, in particular, on the anisotropy of the thermal expansion of an alloy in the region of the martensitic transformation.

2. EXPERIMENTAL

The Ni–Mn–Ga Heusler alloy was melted by argon–arc melting from the high-purity metals and,

then, it was subjected to additional vacuum remelting. The complication of the method of producing the alloy by additional remelting is due to the specific feature of arc melting that, during crystallization of the melt in a copper water-cooled crucible, crystals grow from the crucible walls forming quite coarse columnar-shaped grains. Near the martensitic transformation temperature, the probability of initiating micro- and macrocracks along the boundaries of such grains sharply increases under action of deformations (internal stresses) caused by the phase transformation. Several macrocracks and many microcracks are, as a rule, observed in the ingots. In this case, the near-surface layers of the ingots also contain micropores that are formed due to the excess gas saturation of the alloy during melting. These defects substantially decrease the already low plasticity of the alloy, leading to a premature fracture of a deformed sample. In addition, the pellet-like shape of the ingot prepared by this melting method substantially hampers the MIF deformation of the alloy. The cylindrical billets are the most suitable in this case. To increase the integrity of the ingot structure and to obtain a suitable shape of the billet shape, the cast alloy melt was poured into a cylindrical quartz cap. Then, the obtained ingot was subjected to additional vacuum remelting in a vacuum of 10^{-3} Pa on heating to 1300°C for the alloy degassing and removing pores that form because of a temperature gradient during pouring the melt into the cup. As a result, we prepared the Heusler alloy ingot with the minimum amount of micropores and with no microcracks. The cylindrical ingot was 16.3 mm in diameter and 13.3 mm in height.

An analysis of the elemental composition of the alloy carried out using an X-Act (Oxford Instruments) energy-dispersive spectrometer showed that the obtained alloy has composition $Ni_{54.1}Mn_{19.6}Ga_{24.6}Si_{1.7}$ (at %). It was stated within the accuracy of the X-ray spectrum studies that there is no liquation of the chemical composition in whole of the ingot.

An analysis of the thermal expansion anisotropy of the alloy in the region of the martensitic transformation was carried out using a dilatometer with a displacement pickup based on a differential transformer. This method also allows one to estimate a potential possible value of the ferromagnetic shape memory effect, since the change in geometric sizes of the sample during the martensitic transformation indicates the existence of a texture in the alloy (metallographic and crystallographic) that plays the main role in the effect value. The measurements were carried out in the temperature range from −150°C to +300°C at heating–cooling rates of 5–10°C/min. The 1 × 1 × 7-mm sample was cut by the electric-spark method. In all the cases, the thermal expansion was measured along the long side of the sample.

The MIF thermomechanical treatment of the alloy was carried out on a Schenck Trebel RMC 100 testing machine. Figure 1a shows the schematic of MIF thermomechanical treatment method. The MIF method consists of subsequent deformation of the sample by upset forging by 15–35% with a sample canting by 90° at each next transition, at least, in three orthogonal directions for the change in the direction of deformation of the material. At the final stage of MIF, the sample drawing was performed, during which the sample was only deformed in two directions to form a crystallographic texture in the alloy.

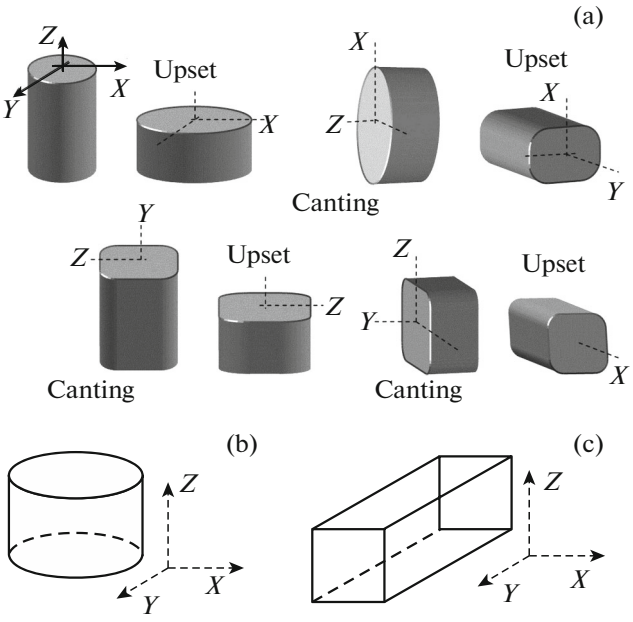

Fig. 1. (a) Scheme of plastic MIF deformation; schematic image and chosen directions of a billet of the polycrystalline $Ni_{54.1}Mn_{19.6}Ga_{24.6}Si_{1.7}$ alloy in (b) as-cast state, and (c) after forging.

The thermomechanical treatment of the alloy by the MIF method was carried out in the temperature range 660–680°C and the strain rates 10^{-4}–5×10^{-4} s^{-1}. The corresponding deformation temperatures were chosen based on an analysis of the temperature–rate conditions of the plastic deformation for the alloys of this system [46–48]. The alloy deformation was performed without a containment shell, taking into account that the oxidation processes in SME alloys at temperatures 600–700°C are not very intense and do not lead to substantial change in the sample microstructure [49, 50].

According to these studies, the optimal temperature of plastic deformation of the Heusler alloys is the range of the phase transformation of the ordered $L2_1$ phase to the disordered $B2$ phase. For the alloy under study, this range is 650–800°C. As a result of remelting of the alloy in the quartz cap and removing an ingot part with a draw, the cylindrical sample for the defor-

mation treatment was a cylinder 16.3 mm in diameter and 13.3 mm in height. The choice of the schematic direction of the sample is shown in Fig. 1b. After 6 upset forging passes and the final drawing, we obtained the deformed sample as an 11 × 11 × 24-mm^3 rectangular parallelepiped (Fig. 1c).

The microstructure of the alloy was studied using a Tescan Mira 3 LMH high-resolution microscope in the regime of registration of back-scattered electrons. This method makes it possible to analyze the structure of a material on a comparatively large area with the resolution of grains to several dozen nanometers. The samples for the studies were cut from the alloy ingot by the electric-spark technique. Thereafter, the cut plane was ground on an abrasive paper and then was subjected to electric polishing in the electrolyte solution with composition 90% butanol + 10% HCl.

3. THERMAL EXPANSION OF THE ALLOY IN AN AS-CAST STATE

To study the anisotropies of the thermal expansion of the polycrystalline alloy in as-cast states, the 1 × 1 × 7-mm samples were cut in two mutually perpendicular directions in the *XOY* plane. The following should be noted. As aforementioned, the vacuum remelting was carried out in a quartz cup. The alloy crystallization (crystal growth) went from the cup walls to its center. In this case, directions *OX* and *OY* are equivalent. Because of this, the first sample was cut so that its long side was parallel to the radius or parallel to the crystal growth ($\|OX$, $\|OY$, since these directions are equivalent) the second sample was cut in the same plane, but its long side was perpendicular to the crystal growth (perpendicularly to the crystal radius).

Figure 2 shows the results of measuring the thermal expansion of both samples on heating and cooling in the temperature range from −100°C to −20°C. The scales along the abscissa axis and the ordinate axis are the same. In all the cases, the thermal expansion was measured along the long side of the sample.

As the first sample was cooled, its length decreased linearly by anharmonic law over the entire temperature range. However, in the temperature range from −73°C to −81°C, the curve demonstrates a stepwise elongation of the sample by 0.06%. This indicates that the direct martensitic transformation occurs in the alloy. As the sample was heated in the temperature range under study, analogous deviation from the anharmonic change in the sample length was observed in the range from −66°C to −59°C. In this case, the sample is stepwise contracted by the same value of 0.06%.

In the case of the second sample, a stepwise change in the geometric sizes of the sample is also observed near the martensitic transformation. The jump is 0.04%, but its direction has the opposite sign, unlike the case of the first sample. That is, the sample stepwise contracted during the direct martensitic transformation in the range from −69°C to −79°C and it is elongated during the inverse transformation in the range from −66°C to −59°C.

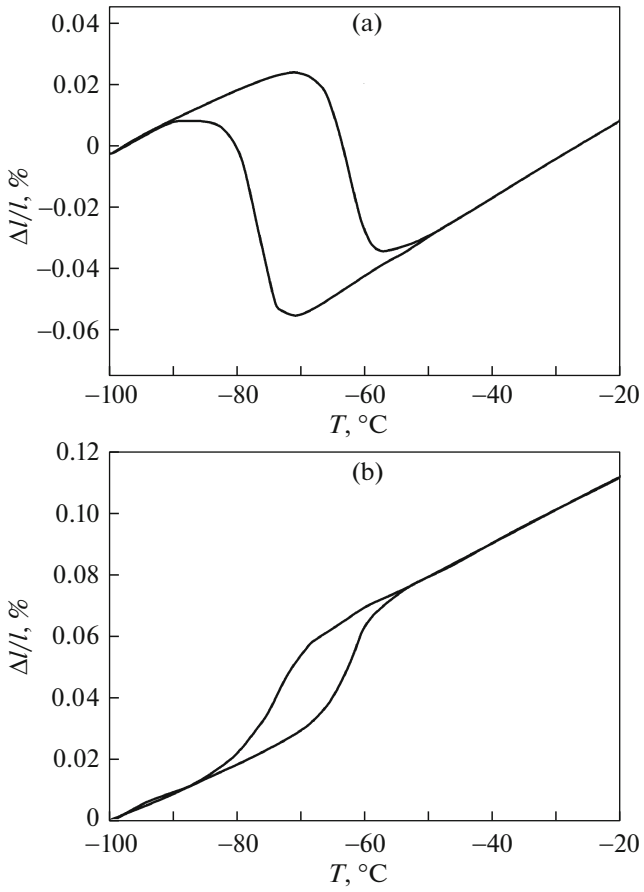

Fig. 2. Temperature dependences of the thermal expansion of the polycrystalline $Ni_{54.1}Mn_{19.6}Ga_{24.6}Si_{1.7}$ alloy in as-cast state measured (a) along the radial component of the billet ($\|OX$, $\|OY$) and (b) perpendicularly to the radial component of the billet.

According to the data on characteristic temperatures of the martensitic transformation, the hysteresis in the as-cast alloy is about 14.5°C. The existence of this relatively small hysteresis during the phase transformation demonstrates a fairly homogeneous alloy structure and the absence of the liquation of the composition. Thus, it is not necessary to subject the alloy to a homogenizing annealing that is a standard procedure for these alloys.

Thus, as a result of crystallization of the melt in a quartz cup, a weak crystallographic texture of growing crystals forms in the alloy that leads to the anisotropy of the thermal expansion in the region of the martensitic transformation.

4. MICROSTRUCTURES OF THE AS-CAST ALLOY AND THE ALLOY AFTER FORGING

The microstructure of the as-cast alloy was studied on a metallographic section in plane *XOY*. Figure 3a presents the corresponding results. The general analysis of the microstructure of the as-cast alloy shows that it does not contain micropores and microcracks corresponding to traditional casting of Heusler alloys. The structure contains equiaxed 100–400-μm grains.

As aforementioned, after 6 upset forging passes and the final drawing, we obtained the deformed sample as a rectangular parallelepiped. The drawing at the final MIF stage (two last passes) was carried out to form a crystallographic texture in the material. As a result, the initial axes of the billet occur as shown in Fig. 1c. Axes *OX* and *OZ* are perpendicular to the drawing axis and must be equivalent to one another. To study the microstructure of the alloy after MIF, we prepared a metallographic section in plane *XOZ*. Figure 3b is the image of the alloy microstructure. Axis *OZ* is horizontal to Fig. 3b. A bimodal "necklace"-type structure formed in the structure as result of the deformation. Quite coarse 100–200-μm grains are surrounded with fine 1–10-μm grains. The existence of a diffuse contrast in coarse grains indicates that a nonequilibrium substructure with high internal stresses formed in them. Figure 3c shows the enlarged magnification of the fine-grained structure. It is seen that the grain contrast is fairly clear, which indicates large-angle grain disorientations formed as a result of the dynamic recrystallization.

It is assumed that this type of the structure will favor the increase in the stability of functional properties of polycrystalline Heusler alloys. To confirm this assumption, it is necessary to carry out the experiment on the study of the alloy properties via the martensite transformation temperature during repeated cycles of heating and cooling.

5. THERMAL EXPANSION OF THE ALLOY AFTER PLASTIC FORGING DEFORMATION

As aforementioned, at the final stage of plastic forging deformation, a so-called drawing was performed to form a crystallographic texture in the billet. In the billet in the form of an elongated rectangular parallelepiped, the drawing axis coincides with direction *OY*. Axes *OX* and *OZ* of the deformed billet are perpendicular to the drawing axis and must be equivalent to one another (*OX* ~ *OZ*). Because of this, to study the anisotropy of the thermal expansion, two samples with a long side along axes *OX* and *OY* were cut. Figure 4 shows the temperature dependence of the thermal expansion measured on heating and cooling of the samples in the temperature range from −100°C to −20°C. The scales along the abscissa axis and the ordinate axis were the same. However, the scale along the ordinate axis is rougher by a factor of two as compared to that in the as-cast state (Fig. 2).

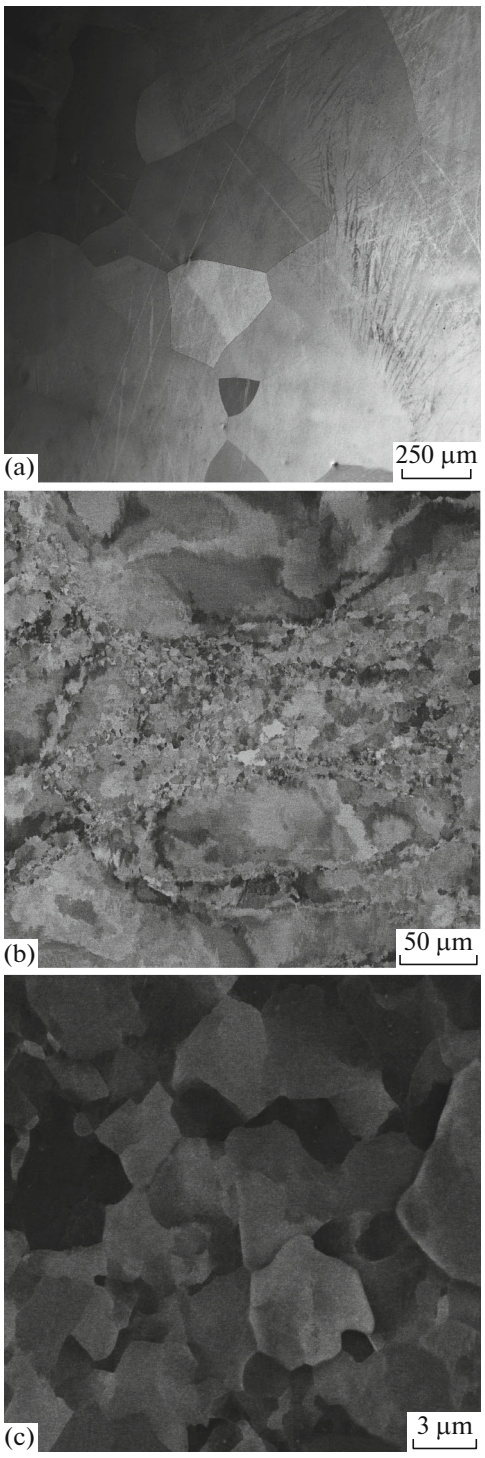

Fig. 3. Microstructure of the polycrystalline $Ni_{54.1}Mn_{19.6}Ga_{24.6}Si_{1.7}$ alloy: (a) in as-cast state, and (b, c) after plastic MIF deformation.

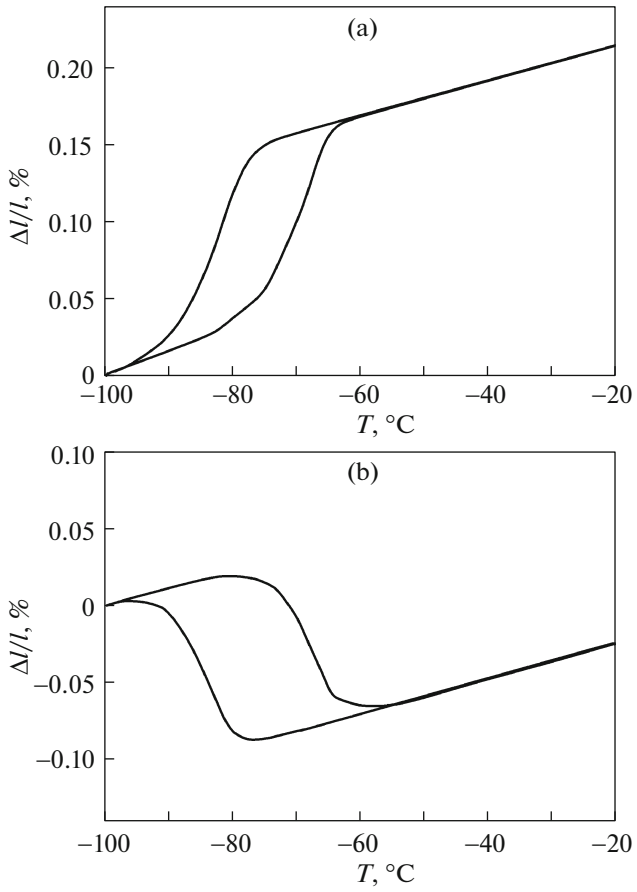

Fig. 4. Temperature dependences of the thermal expansion of the polycrystalline $Ni_{54.1}Mn_{19.6}Ga_{24.6}Si_{1.7}$ alloy after plastic forging deformation: (a) crosswise the drawing axis ($\|OX$) and (b) along the drawing axis ($\|OY$).

Figure 4a shows the curves of heating and cooling of the sample cut transversely to the drawing axis ($\|OX$).

As in the case of the as-cast state, the sample length is changed by an anharmonic law behind the range of the temperatures of martensitic transformation. The sample stepwise contracts by 0.13% during the direct martensitic transformation and elongates by this value during the inverse transformation. The characteristic transformation temperatures are as follows: $M_S = -78°C$, $M_F = -90°C$, $A_S = -76°C$, and $A_F = -65°C$. As for the second sample that was cut along the drawing axis, it, conversely, stepwise elongates and contracts by 0.12% during the direct and inverse transformation, respectively. The characteristic transformation temperatures are as follows: $M_S = -79°C$, $M_F = -92°C$, $A_S = -75°C$, and $A_F = -63°C$. In this case, the phase transformation hysteresis is 15°C.

As a result of the plastic deformation of the alloy by the method of the multiple isothermal forging, the characteristic martensitic transformation temperatures shift to lower temperatures by 6–11°C. Such a behavior is characteristic for this subject of the studies, since it is due to hampering the motion in the deformed structure of transformation dislocations that are martensite steps of atomic sizes at interfaces.

In the initial billet, direction *OX* coincided with the radial component of the billet, and the sample cut along this direction elongated during the direct martensitic transformation. As a result of the forging of the alloy, the initial texture of the crystal growth was suppressed and the replacement of the deformation for the texture. Now, conversely, the sample contracts during the direct transformation, unlike the as-cast sample. In the samples cut along direction *OY*, the character of stepwise change in the length is the same in both structural states (as-cast and forged). However, the deformed sample demonstrated two-fold increase in the jump value.

Thus, the thermomechanical treatment of the polycrystalline Heusler alloy by multiple isothermal forging leads to formation of the anisotropy of physical properties, in particular, the anisotropy of the thermal expansion in the region of the martensitic transformation. It should be noted that the increases in the anisotropy and the absolute value of the stepwise change in the geometric sizes of the forged sample during the phase transformation are not very significant. In a number of cases, the texture of the crystal growth in Heusler alloy ingots gives slightly high values of the elongation. Because they were the first experiments on treatment of Heusler alloys by multiple isothermal forging, the number of the passes during forging was minimized to study the microstructure at the initial stages of the deformation. Since the formation of the texture at the final stage of deformation (drawing) was performed one time. In further experiments, the texture and the anisotropy can be significantly increased by increase in the number of passes during drawing and formation of more elongated billet.

6. CONCLUSIONS

In the polycrystalline $Ni_{54.1}Mn_{19.6}Ga_{24.6}Si_{1.7}$ (at %) alloy after casting and subsequent vacuum remelting in a quartz cup, a weak texture forms as a result of predominant crystal growth from the cup walls to its center. This leads to the thermal expansion anisotropy of the alloy near the martensitic transformation. The sample stepwise elongates in the direction of the crystal growth during the direct martensitic transformation. In the transverse direction, the elongation is changed by stepwise decrease in the length.

The multiple isothermal forging was applied to Heusler alloys for the first time. As a result of the plastic forging deformation, a bimodal structure forms; the structure is coarse 100–200 μm grains surrounded by the fine-structure with 1–10 μm grain size. It is assumed that this structural type will favor the increase in the thermal stability of functional properties of the

alloy as a result of repeated cycles of the martensitic transformation.

To form the crystallographic texture and to increase the internal stresses in the alloy under study, the alloy was subjected to drawing at the final stage of forging. This led to the change in the anisotropy vector and the increase in the effect. The analysis of the thermal expansion near the martensitic transformation showed that the sample cut transversely to the drawing axis stepwise contracted as a result of the direct martensitic transformation and the sample cut along the axis stepwise elongated.

ACKNOWLEDGMENTS

This work was supported by the Russian foundation for Basic Research (project no. 16-32-60159 mol_a_dk) (for I.I. Musabirov). The study of the microstructure and the deformation treatment of the alloy were performed using equipment of the Collective Use Center "Structural and Physicomechanical Studies of Materials" of the Institute of Metal Superplasticity Problems of RAS.

REFERENCES

1. E. Pagounis, R. Chulist, M. J. Szczerba, and M. Laufenberg, Appl. Phys. Lett. **105**, 052405 (2014).
2. V. A. Chernenko, J. M. Barandiaran, V. A. Lvov, J. Gutierrez, P. Lazpita, and I. Orued, J. Alloys Compd. **577**, S305 (2013).
3. V. D. Buchelnikov, V. V. Khovailo, and T. Takagi, J. Magn. Magn. Mater. **300**, e459 (2006).
4. U. Gaitzsch, J. Romberg, M. Pötschke, S. Roth, and P. Müllner, Scr. Mater. **65**, 679 (2011).
5. A. Sozinov, A. A. Likhachev, N. Lanska, and K. Ullakko, Appl. Phys. Lett. **80**, 1746 (2002).
6. I. I. Musabirov, Kh. Ya. Mulyukov, V. V. Koledov, and V. G. Shavrov, Tech. Phys. **56**, 423 (2011).
7. Yu. V. Kaletina and E. G. Gerasimov, Phys. Solid State **56**, 1634 (2014).
8. Kh. Ya. Mulyukov, I. I. Musabirov, and A. V. Mashirov, Pis'ma Mater. **2**, 194 (2012).
9. V. D. Buchelnikov and V. V. Sokolovskiy, Phys. Met. Metallogr. **112**, 633 (2011).
10. A. P. Kamantsev, V. V. Koledov, A. V. Mashirov, E. T. Dilmieva, V. G. Shavrov, J. Cwik, A. S. Los, V. I. Nizhankovskii, K. Rogacki, I. S. Tereshina, Yu. S. Koshkidko, M. V. Lyange, V. V. Khovaylo, and P. Ari-Gur, J. Appl. Phys. **117**, 163903 (2015).
11. A. Zhukov, V. Rodionova, M. Ilyn, A. M. Aliev, R. Varga, S. Michalik, A. Aronin, G. Abrosimova, A. Kiselev, M. Ipatov, and V. Zhukova, J. Alloys Compd. **575**, 73 (2013).
12. V. V. Sokolovskiy, R. R. Fayzullin, V. D. Buchelnikov, M. O. Drobosyuk, and V. V. Khovaylo, J. Magn. Magn. Mater. **343**, 6 (2013).
13. R. Fayzullin, V. Buchelnikov, M. Drobosyuk, A. Mashirov, A. Kamantsev, B. Hernando, M. Zhukov, V. Koledov, and V. Shavrov, Solid State Phenom. **233–234**, 183 (2015).
14. E. Pagounis, M. J. Szczerba, R. Chulist, and M. Laufenberg, Appl. Phys. Lett. **107**, 152407 (2015).
15. M. Pötschke, S. Weiss, U. Gaitzsch, D. Cong, C. Hurrich, S. Roth, and L. Schultz, Scr. Mater. **63**, 383 (2010).
16. F. Albertini, L. Morellon, P. A. Algarabel, M. R. Ibarra, L. Pareti, Z. Arnold, and G. Calestani, J. Appl. Phys. **89**, 5614 (2001).
17. U. Gaitzsch, J. Romberg, M. Pötschke, S. Roth, and P. Müllner, Scr. Mater. **65**, 679 (2011).
18. I. I. Musabirov, R. R. Mulyukov, and V. V. Koledov, IOP Conf. Ser.: Mater. Sci. Eng. **82**, 012064 (2015).
19. S. Taskaev, V. Buchelnikov, M. Ulyanov, D. Bataev, V. Khovaylo, A. Usenko, M. Lyange, K. Skokov, O. Gutfleisch, A. Pellenen, and D. Karpenkov, J. Appl. Phys. **117**, 123914 (2015).
20. D. R. Nugmanov, O. Sh. Sitdikov, and M. V. Markushev, Pis'ma Mater. **7**, 198 (2017).
21. S. N. Sergeev, I. M. Safarov, A. V. Korznikov, R. M. Galeev, S. V. Gladkovskii, and D. A. Dvoinikov, Pis'ma Mater. **5**, 48 (2015).
22. R. Ya. Lutfullin, M. Kh. Mukhametrakhimov, P. A. Klassman, and V. V. Astanin, Perspekt. Mater. **15**, 66 (2013).
23. E. V. Avtokratova, O. E. Mukhametdinova, O. Sh. Sitdikov, and M. V. Markushev, Pis'ma Mater. **5**, 129 (2015).
24. R. A. Gaisin, V. M. Imaev, R. M. Imaev, and E. R. Gaisina, Pis'ma Mater. **5**, 124 (2015).
25. S. V. Krymskii, D. K. Nikiforova, M. Yu. Murashkin, and M. V. Markushev, Perspekt. Mater. **12**, 387 (2011).
26. I. Sh. Valeev, A. Kh. Valeeva, R. R. Mulyukov, and R. Kh. Khisamov, Pis'ma Mater. **6**, 347 (2016).
27. R. R. Mulyukov, Ross. Nanotekhnol. **2** (7–8), 38 (2007).
28. O. Sh. Sitdikov, Perspekt. Mater. **9**, 5 (2015).
29. O. E. Mukhametdinova, R. N. Garipova, E. V. Avtokratova, and O. Sh. Sitdikov, Fundam. Probl. Sovrem. Materialoved. **13**, 249 (2016).
30. R. M. Galeev, O. R. Valiakhmetov, G. F. Khasanova, and R. R. Mulyukov, Perspekt. Mater. **15**, 40 (2013).
31. Y. Dai, L. Hou, Y. Fautrelle, Z. Li, C. Esling, Z. Ren, and X. Li, Mater. Des. **134**, 469 (2017).
32. J. Liu, J. Wang, H. Zhang, C. Jiang, and H. Xu, J. Alloys Compd. **541**, 477 (2012).
33. B. Lu, H. B. Wang, Y. Liu, J. X. Liu, and H. L. Wang, Trans. Nonferr. Met. Soc. China **16**, 843 (2006).
34. S. Besseghini, E. Villa, F. Passaretti, M. Pini, and F. Bonfanti, Mater. Sci. Eng. A **378**, 415 (2004).
35. R. Chulist, M. Potschke, A. Boehm, H.-G. Brokmeier, U. Garbe, T. Lippmann, C.-G. Oertel, and W. Skrotzki, MRS Proc. **1050**, BB09-03 (2007).
36. A. Böhm, S. Roth, G. Naumann, W. G. Drossel, and R. Neugebauer, Mater. Sci. Eng. A **481–482**, 266 (2008).
37. H. Morawiec, T. Goryczka, A. Drdzen, J. Lelatko, and K. Prusik, Solid State Phenom. **154**, 133 (2009).

38. N. I. Kourov, A. V. Korolev, V. G. Pushin, and E. V. Marchenkova, Phys. Solid State **54**, 2128 (2012).
39. R. Chulist, W. Skrotzki, C.-G. Oertel, A. Böhm, T. Lippmann, and E. Rybacki, Scr. Mater. **62**, 650 (2010).
40. R. Chulist, A. Bohm, E. Rybacki, T. Lippmann, C.-G. Oertel, and W. Skrotzki, Mater. Sci. Forum **702–703**, 169 (2012).
41. I. I. Musabirov, I. Z. Sharipov, and R. R. Mulyukov, Russ. Phys. J. **58**, 745 (2015).
42. I. I. Musabirov, I. M. Safarov, I. Z. Sharipov, R. R. Mulyukov, A. V. Mashirov, and V. V. Koledov, Zh. Radioelektron., No. 1, 11 (2015).
43. D. Y. Cong, Y. D. Wang, R. L. Peng, P. Zetterström, X. Zhao, P. K. Liaw, and L. Zuo, Metall. Mater. Trans. A **37**, 1397 (2006).
44. D. Y. Cong, Y. D. Wang, P. Zetterström, R. L. Peng, R. Delaplane, X. Zhao, and L. Zuo, Mater. Sci. Technol. **21**, 1412 (2005).
45. R. Chulist, W. Skrotzki, C.-G. Oertel, A. Böhm, H.-G. Brokmeier, and T. Lippmann, Int. J. Mater. Res. **103**, 575 (2012).
46. I. I. Musabirov, I. M. Safarov, M. I. Nagimov, I. Z. Sharipov, V. V. Koledov, A. V. Mashirov, A. I. Rudskoi, and R. R. Mulyukov, Phys. Solid State **58**, 1605 (2016).
47. I. I. Musabirov, I. M. Safarov, I. Z. Sharipov, M. I. Nagimov, V. V. Koledov, V. V. Khovailo, and R. R. Mulyukov, Phys. Solid State **59**, 1570 (2017).
48. I. Musabirov, I. Safarov, M. Nagimov, I. Sharipov, V. Koledov, V. Khovailo, and R. Mulyukov, Mater. Today: Proc. **4**, 4851 (2017).
49. M. Kök, G. Pirge, and Y. Aydogdu, Appl. Surf. Sci. **268**, 136 (2013).
50. M. Kök and K. Yildiz, Appl. Phys. A **116**, 2045 (2014).

Translated by Yu. Ryzhkov